PCCP

PAPER

View Article Online
View Journal | View Issue

Cite this: *Phys. Chem. Chem. Phys.*, 2025, **27**, 23612

How could ratiometric thermometry with thermally activated delayed fluorescent (TADF) emitters practically work?

Markus Suta

Luminescence is a temperature-dependent phenomenon. That fundamental property can be used to gain information about the local temperature around a phosphor, which resulted in the development of luminescence thermometry. While this remote temperature sensing technique has gained extensive interest within the field of inorganic phosphors, thermally activated delayed fluorescent (TADF) emitters have so far only been scarcely considered for this application. Within this work, guidelines on the most effective usage of TADF emitters as potential luminescent thermometers are elaborated and what sets them apart from alternative inorganic emitters. It is demonstrated that the dynamic working range of such conceptualized thermometers is dominated by the interplay between the (reverse) intersystem crossing and the radiative decay constants of the emissive states of interest. Pioneering foundations laid by Christel Marian's group are decisive in a more fundamental understanding of the design of such emitters for luminescence thermometry.

Received 3rd July 2025,
Accepted 20th October 2025

DOI: 10.1039/d5cp02539g

rsc.li/pccp

Introduction

Luminescence has always been a temperature-dependent phenomenon and it comes as no surprise that there has been an increasing interest in its use for thermometry purposes. Among the simplest and practically appealing approaches is self-referenced ratiometric thermometry,[1,2] in which the luminescence intensity ratio (LIR) of thermally coupled, radiatively emitting excited states from the same electron configuration serves as a temperature measure. For intraconfigurational levels with no offset in their equilibrium configurational coordinates, Boltzmann's law strictly holds as a governing calibration law based on the underlying nonradiative multiphonon transitions.[3] The energy splitting between thermally coupled electronic states should be ideally in the order of the thermal energy k_BT to be probed (k_B is Boltzmann's constant) for a population ratio in the order of 1 (normalized per microstate). Especially trivalent lanthanoid ions with their intraconfigurational, narrow-line $4f^n \leftrightarrow 4f^n$ transitions ($n = 2$ for Pr^{3+} to $n = 12$ for Tm^{3+}) in the ultraviolet (UV), visible, and near infrared (NIR) range are naturally suited for that purpose because the low linewidth of the related emission lines allows to spectrally resolve such low energy gaps.[4] Besides those intraconfigurational transitions, also emitters with interconfigurational, broad-banded $4f^n \leftrightarrow 4f^{n-1}5d^1$ transitions such as Sm^{2+} ($n = 6$) or Pr^{3+} ($n = 2$) have gained more interest as they offer a way for very sensitive thermal response exploiting very large energy gaps.[5–13] Finally, also the $3d^3$ ion Cr^{3+} falls into that category as thermal coupling between its excited $^2E_g(^2G)$ ($(t_{2g})^3$ configuration in an octahedral field) and $^4T_{2g}(^4F)$ ($(t_{2g})^2(e_g)^1$ configuration in an octahedral field) states is similarly effective and their mutual energy gap can be tuned by the ligand field strength.[14–24] In all of those latter cases, a configurational crossover is explicitly used that follows Boltzmann behavior under specific conditions as well (see also below).[6,25] It should be noted, however, that while crossover thermometry is a kinetically feasible possibility to boost the relative sensitivity, $S_r(T)$, it does not necessarily increase the overall achievable precision, which still relies on thermodynamics and requires an almost equalized population ratio per microstate for appreciable signal-to-noise. For optimal thermodynamically motivated precision, several conditions have been recently established.[3,26]

Besides those single-ion emitters, an alternative class of molecular luminophors that have recently (re-)gained enormous attention are thermally activated delayed fluorescent (TADF) emitters.[27] Although this effect was originally established on $[UO_2]^{2+}$ salts by Perrin in 1929,[28] and later reobserved by Lewis *et al.*,[29] the first detailed kinetic study was performed by Parker and Hatchard in 1961 on Eosin Y.[30,31] A major breakthrough was achieved by Adachi's group in 2012 when it demonstrated the potential of such emitters for

Inorganic Photoactive Materials, Institute of Inorganic Chemistry, Heinrich Heine University Düsseldorf, Universitätsstraße 1, 40225 Düsseldorf, Germany.
E-mail: markus.suta@hhu.de

electroluminescent organic light-emitting diodes (OLEDs) without the explicit necessity of heavy metals and the possibility to harvest singlet-based emission with a theoretical internal quantum yield of 100%.[31] While Adachi's class of emitters relied on classic donor-acceptor systems with strong charge transfer (CT)-type emission,[32–35] Hatakeyama *et al.* originally introduced a class of so-called multiresonant (MR)-type TADF emitters that show narrower emission, especially in the blue range.[36–41] In all those emitters, it is generally recommended that $\Delta E_{21} \sim k_B T$ for effective TADF. While this is thermodynamically clearly reasonable, it is often argued that otherwise reverse intersystem crossing (rISC) could not occur that is necessary to thermally populate the excited singlet state. It is important to note that there are also examples reported in literature, for which (r)ISC at room temperature can be unusually fast, however.[34,42,43] Several mechanisms exist that can render the coupling between an excited singlet and triplet state stronger. One of the earliest findings in that regard were El-Sayed's rules stating that spin–orbit mediated intersystem crossing may occur more easily in organic systems if there is a compensating change in the orbital type during a nonradiative transition accompanied by a change of the total spin.[44] By virtue of this rule, it becomes evident why ISC is particularly fast in many aromatic ketones despite the absence of heavier atoms that otherwise often enable spin–orbit coupling. In many TADF emitters, however, the connected excited singlet and triplet states have strong CT-type character with a much more delocalized charge density distribution. El-Sayed's rules then set a reasonable foundation why (r)ISC between the relevant singlet and triplet states of TADF emitters is expectedly only weak.[45] There are several mechanisms that allow conventional spin–orbit coupling beyond a simple heavy-atom effect such as spin-vibronic and vibrational spin–orbit coupling that can enhance intrinsic ISC as well.[46–53] In many of those mechanisms, the density of excited triplet states or the presence of states with localized electron density play a crucial role. In addition, a fundamental mechanistic understanding requires consideration of spin–orbit coupling beyond the Franck–Condon coupling scheme. In fact, many of these more sophisticated approaches to (r)ISC have been thoroughly investigated by Christel Marian's group, whom this work is also dedicated to. Overall, those rules prove useful together with the comparison to common inorganic emitters to elucidate what conditions organic TADF emitters need to fulfil to be useful as ratiometric luminescent thermometers at all, as only few works highlight the potential use of those emitters in the context of optical temperature sensing at all.[54–58]

Within this work, I will compare the two possibilities of ratiometric thermometry using steady-state spectroscopy and an alternative time-resolved concept. Several limiting cases will be discussed that allow to embed the different emitters into a generalized scheme for luminescent thermometry. It will be considered how the various approaches to enhance intrinsic coupling between an excited singlet and triplet state could help tailor TADF emitters for luminescence thermometry and what natural limitations this class of emitters faces for that application compared to inorganic emitters.

Results and discussion

Assumptions

In order to analyze the thermometric potential of a classic TADF emitter, we will assume a simplified energy level scheme as depicted in Fig. 1 for the discussion. Excitation occurs into any continuum of auxiliary states $\{|a\rangle\}$, from which fast nonradiative relaxation into the two relevant, thermally coupled excited singlet $S_1 = |2\rangle$ and triplet states $T_1 = |1\rangle$ occurs. It is noteworthy that there are practical cases, in which there may be an inverted singlet–triplet gap[43] or which are not fully accurately described by this simplistic two-excited state model.[46–53] Moreover, no additional specification about the explicit nature of the states (localized, CT-type) is preliminarily assumed, which can have, however, an impact on the actual spectral appearance and also the intersystem crossing rates. Those specific cases will be discussed below once the preliminary analysis is set.

Steady-state conditions and ratiometric thermometry in the frequency domain. The set of coupled rate equations results in the following general steady-state solution for the intensity ratio of the two emissive states two thermally coupled excited states nonradiative fed by an excited auxiliary state $|a\rangle$[3,59]

$$R_{21}(T) = \frac{I_{20}(T)}{I_{10}(T)} = C\frac{\alpha_{a2}k_1 + k_{nr}^{abs}(T)}{\alpha_{a1}k_2 + k_{nr}^{em}(T)} \quad (1)$$

with C as electronic pre-factor connected to the spontaneous emission rates A_{20} and A_{10} for the radiative transitions $|2\rangle \rightarrow |0\rangle$ and $|1\rangle \rightarrow |0\rangle$,

$$C = \frac{A_{20}}{A_{10}} = \frac{\beta_{20}k_{2r}}{\beta_{10}k_{1r}} \quad (2)$$

where β_{20} and β_{10} are the branching ratios of the respective transitions and k_2 and k_1 are the (experimentally accessible) total radiative decay rates of the excited levels $|2\rangle$ and $|1\rangle$. In the context of TADF emitters, it is usually $\beta_{10} = \beta_{20} = 1$ and $k_{jr} = k_j\phi_j$ ($j = 1, 2$). The coefficients α_{aj} ($j = 1, 2$) denote feeding ratios

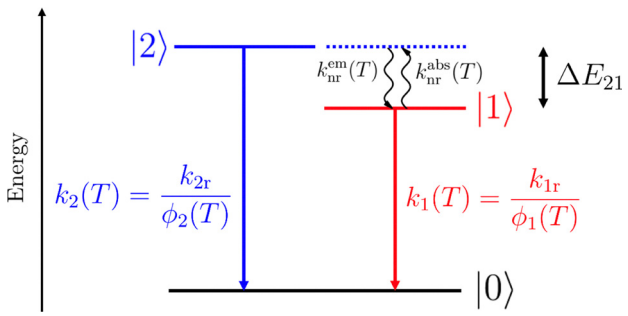

Fig. 1 Simplified underlying three-level scheme with two thermally coupled excited states separated by an energy gap ΔE_{21} that is used as a model system in this work. In the case of a TADF emitter, $|1\rangle = T_1$ is the excited triplet and $|2\rangle = S_1$ the excited singlet state. The non-radiative transition rates governing the thermal coupling between the excited states then describe ISC ($k_{nr}^{em}(T) = k_{ISC}(T)$) and reverse ISC ($k_{nr}^{abs}(T) = k_{rISC}(T)$). The two states are characterized by total decay rate constants $k_1 = k_{1r}/\phi_1$ and $k_2 = k_{2r}/\phi_2$ with $\phi_{1,2}$ as the internal (eventually temperature-dependent) quantum yields.

from the auxiliary state. Since the potential energy curves of the excited singlet and triplet states usually have different equilibrium geometries, they will necessarily cross in a configurational coordinate space. In that limit, the temperature dependence of the nonradiative rate constants can be approximated by an Arrhenius-type law,

$$k_{\mathrm{nr}}^{\mathrm{em}}(T)(=k_{\mathrm{ISC}}(T)) = g_1 k_{\mathrm{nr}}(0)\exp\left(-\frac{\Delta E_{X2}}{k_{\mathrm{B}}T}\right) \quad (3)$$

with g_1 as the degeneracy of the lower excited state (usually g_1 = 3 for a T_1 state), $k_{\mathrm{nr}}(0)$ as an intrinsic coupling strength and ΔE_{X2} as the barrier between the zero-point energy of the excited singlet state and the crossover point X. Very often is $\Delta E_{\mathrm{X2}} \ll k_{\mathrm{B}}T$ in the regarded temperature range and that temperature dependence can be neglected ($k_{\mathrm{nr}}^{\mathrm{em}}(T) \simeq g_1 k_{\mathrm{nr}}(0)$). The corresponding absorption rate $k_{\mathrm{nr}}^{\mathrm{abs}}(T)$ is analogously given by

$$k_{\mathrm{nr}}^{\mathrm{abs}}(T)(=k_{\mathrm{rISC}}(T)) = g_2 k_{\mathrm{nr}}(0)\exp\left(-\frac{\Delta E_{X1}}{k_{\mathrm{B}}T}\right) \quad (4)$$

with ΔE_{X1} as the barrier between the potential energy curve of the excited triplet state and the crossover to the excited singlet state potential energy curve. Using eqn (2)–(4), we can rearrange eqn (1) and obtain

$$R_{21}(T) = \frac{\frac{\alpha_{a2}}{\phi_1}}{\frac{\alpha_{a1}}{\phi_2} + \frac{g_1 k_{\mathrm{nr}}(0)}{k_{2\mathrm{r}}}\exp\left(-\frac{\Delta E_{X2}}{k_{\mathrm{B}}T}\right) + \frac{\frac{g_2 k_{\mathrm{nr}}(0)}{k_{1\mathrm{r}}}\exp\left(-\frac{\Delta E_{X1}}{k_{\mathrm{B}}T}\right)}{\frac{\alpha_{a1}}{\phi_2} + \frac{g_1 k_{\mathrm{nr}}(0)}{k_{2\mathrm{r}}}\exp\left(-\frac{\Delta E_{X2}}{k_{\mathrm{B}}T}\right)}} \quad (5)$$

It is insightful to consider the limiting case $\Delta E_{X2} \ll k_{\mathrm{B}}T$, *i.e.* the assumption of a temperature-independent non-radiative emission rate constant (see eqn (3)). In addition, it is useful to consider the limit of efficient nonradiative coupling ($k_{\mathrm{nr}}(0) > k_{1\mathrm{r}}$, $k_{2\mathrm{r}}$). Under these assumptions, eqn (5) evolves to the approximation

$$R_{21}(T) \approx B + C\frac{g_2}{g_1}\exp\left(-\frac{\Delta E_{21}}{k_{\mathrm{B}}T}\right) \quad (6)$$

with C as defined in eqn (2) and

$$B \approx \frac{\alpha_{a2} k_{2\mathrm{r}}}{g_1 k_{\mathrm{nr}}(0)\phi_1} \quad (7)$$

This is a situation that occurs for various inorganic emitters showing both broad-band and narrow-line emission such as Cr^{3+} ($^4T_{2g}(^4F) \leftrightarrow {}^2E_g(^2G)$, $^2T_{1g}(^2G)$ crossover), Pr^{3+} ($4f^15d^1 \leftrightarrow 4f^2$ crossover), or Sm^{2+} ($4f^55d^1 \leftrightarrow 4f^6$ crossover).[5–23] In all those cases, intrinsic nonradiative coupling $k_{\mathrm{nr}}(0)$ between the indicated excited states (not necessarily intersystem crossing) is indeed much faster ($k_{\mathrm{nr}}(0) \sim \mathrm{ns}^{-1}$) than any of the radiative decay processes ($k_{\mathrm{jr}} \sim \mu\mathrm{s}^{-1} \ldots \mathrm{ms}^{-1}$).[25] Out of that reason, also higher energy gaps ($\Delta E_{21} \gg k_{\mathrm{B}}T$) can be bridged at moderate temperatures already. The population ratio of the two involved excited states, however, may still be very low according to the ratio $k_{\mathrm{nr}}^{\mathrm{abs}}(T)/k_{\mathrm{nr}}^{\mathrm{em}}(T)$, see (eqn (6)), which affects the overall precision of a ratiometric thermometer by means of a low signal-to-noise ratio from the higher energetic emission.

In TADF emitters, however, the situation changes as the intrinsic intersystem crossing rate constant $k_{\mathrm{nr}}(0) = k_{\mathrm{ISC}}(0)$ can become similar to or even lower than the radiative decay rate constant $k_{2\mathrm{r}}$ of an excited singlet state $S_1 = |2\rangle$ (very often, it is $k_{\mathrm{ISC}}(0) < 10\ \mu\mathrm{s}^{-1}$, while $k_{2\mathrm{r}} \sim 100\ \mu\mathrm{s}^{-1}$).[27] In that case, approximation (6) breaks down and the intensity ratio between fluorescence and phosphorescence may not serve a thermometric purpose – the two states are essentially decoupled. Several governing rules have, however, been established as guidelines how (intrinsic) intersystem crossing can be enhanced. Besides the use of heavy atoms and the impact on spin–orbit coupling, El-Sayed's rules offer an alternative way to provoke a spin conversion connected to a simultaneous change in the orbital type for overall total angular momentum conservation.[44] This is encountered in aromatic ketones, for example, in which the lowest energetic triplet states typically have $^3n\pi^*$ character, while the excited singlet states have more dominant $^1\pi\pi^*$ character.[53] Also d^{10} coinage metals (Cu(I), Ag(I), Au(I)) in N-heterocyclic carbene (NHC) complexes can mediate ISC by a combination of a heavy-atom effect together with El-Sayed's rules.[53,60–63] Apart from these two combinations, also spin-vibronic (Herzberg–Teller-type), vibrational spin–orbit, spin–spin, and even hyperfine coupling schemes are known to result in appreciable ISC.[50,53]

A peculiar situation for organic emitters is that strong intersystem crossing can potentially also indirectly affect the radiative decay rate of the excited singlet state, $k_{2\mathrm{r}}$. In contrast to common textbook knowledge, which often states that fluorescence is related to decay times in the order of a few ns, there are also cases, in which (prompt) fluorescence may rather decay in the order of only 0.1–1 μs (*e.g.* in Cu(I) carbene complexes).[53,60–63] In that limit, ISC is similarly fast or even faster than fluorescent decay. The foundations of approximation (6) can then be fulfilled and a high S_1–T_1 energy gap ΔE_{21} may be exploited for sensitive ratiometric thermometry. This is particularly crucial for organic emitters, which usually give rise to broad emission bands. If the energy gap between the coupled excited singlet and triplet state is too low ($\Delta E_{21} \sim k_{\mathrm{B}}T$), there is significant spectral overlap between the two related emission bands, which compromises the overall achievable precision of such a temperature read-out concept. Thus, the S_1–T_1 energy gap needs to be higher than the sum of the effective half widths $\frac{1}{2}\sigma$ of the fluorescence ($\frac{1}{2}\sigma_{\mathrm{fl}}$) and phosphorescence ($\frac{1}{2}\sigma_{\mathrm{ph}}$) emission bands, $\Delta E_{21} > \frac{1}{2}(\sigma_{\mathrm{fl}} + \sigma_{\mathrm{ph}})$ for sufficient spectral resolution in steady-state spectra. In order to make that concept also a precise measure, it should be ideally $R_{21}(T) \sim 1$ in the Boltzmann regime. With $k_{2\mathrm{r}} \sim 10\ \mu\mathrm{s}^{-1}$ and $k_{1\mathrm{r}} \sim 10\ \mathrm{ms}^{-1}$, we can estimate a recommendable $\Delta E_{21} \approx (3\ln 10)k_{\mathrm{B}}T \approx 6.91 k_{\mathrm{B}}T$ for ratiometric thermometry with an organic emitter showing both fluorescence and phosphorescence. According to eqn (4), the corresponding nonradiative absorption rate assuming a negligible crossover barrier ΔE_{X2} (*i.e.* $\Delta E_{X1} \approx \Delta E_{21}$) will be around $k_{\mathrm{nr}}^{\mathrm{abs}}(T) \approx 10^{-3} \times k_{\mathrm{nr}}(0)$ in that case. For kinetically

enabled ratiometric thermometry, it has to be ensured, however, that this nonradiative absorption rate (or rISC) is faster than the total decay $k_1 = k_{1r}/\phi_1$ from the excited T_1 state at the temperature of interest, *i.e.* $k_{nr}^{abs}(T) > k_1$. This last requirement can become problematic in practice as phosphorescence is generally prone to additional nonradiative deactivation processes – especially at ambient conditions in solution and for very broad-banded, Stokes-shifted phosphorescence in the red range. Secondly, strong direct ISC from S_1 to T_1 can also intrinsically enhance the radiative decay rate of the T_1 state, as is known from phosphorescent emitters containing heavy atoms such as Ir(III) or Ru(II) complexes.[64]

It can be concluded that ratiometric thermometry in the spectral or frequency domain will only work with an organic emitter showing sufficiently narrow fluorescent emission that stems from an excited singlet state S_1 strongly coupled to a triplet state T_1 by ISC. It has to be guaranteed that the T_1 decay rate is sufficiently low (ideally, $k_1 \sim 10\ ms^{-1}$) to make rISC a competitive process for thermalization at room temperature. While this can be ensured for most inorganic emitters as described above, this is a common problem with a directly coupled S_1–T_1 pair, in which $k_{nr}(0)$ is often comparable in magnitude compared to k_{1r} or k_{2r}. A more recommendable energy level diagram that could potentially circumvent that dilemma is the one depicted in Fig. 2, which relies on TADF between an excited singlet and triplet state but contains an additional lower energetic more localized triplet state that gives rise to spectrally resolved phosphorescence. However, the nonradiative transition rates have to be carefully adjusted to enable a ratiometric thermometry concept in a spectral or frequency domain. Aromatic ketones such as xanthone, anthrone, fluorenone, or benzophenone could be interesting candidates for that purpose that fulfil many of the indicated criteria.[53,65] Alternatively, metal-containing Zn(II)-based complexes showing TADF may also feature many desirable properties in that regard.[66–70] Ideally, the considered molecule can be pumped into a well-absorbing (delocalized or extended) $^1\pi\pi^*$ state quickly relaxing to a more local $S_1 = {}^1n\pi^*$ state. According to El-Sayed's rules,[44] the coupled triplet state should be dominantly $^3\pi\pi^*$ in nature for fast intrinsic ISC and ultimately relax to a more localized $T_1 = {}^3n\pi^*$ state, from which phosphorescence with high quantum yield could be detected. This is, however, a challenging task to achieve in practice given the fact that $n\pi$ states may be often raised in their energies in case of *e.g.* hydrogen bonding or solvent interactions.[71–83] In addition, it is mandatory that rISC can compete with internal conversion between the excited triplet states and decay of the T_1 state, $k_{rISC}(T) \gtrsim k_{IC}(T_n \rightarrow T_1) + k_1$.

It becomes evident from this literature survey and the number of necessary, partially very harsh assumptions that ratiometric thermometry with TADF emitters (both CT- and MR-type) in the spectral or frequency domain is generally challenging, if not even almost impractical. In the following, it will thus be investigated under what conditions a time-domain ratiometric thermometry approach may be feasible.

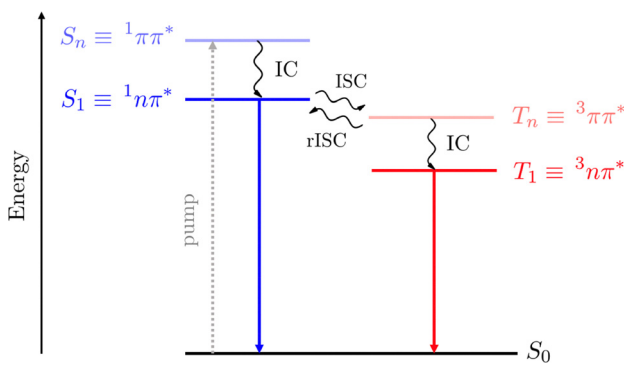

Fig. 2 Recommendable energy level scheme for an organic emitter that may be used as a ratiometric luminescent thermometer in the spectral domain employing steady-state spectra under certain conditions (see text for details on conditions). Nonradiative transitions are denoted as curvy arrows, while radiative transitions are represented by solid arrows. It turns out that this scheme is an oversimplification for many practical organic dyes.

Ratiometric thermometry in the time domain

A major obstacle in ratiometric thermometry of organic (TADF) emitters in the spectral or frequency domain (*i.e.* from steady-state spectra) is the broad-banded nature of both fluorescent and phosphorescent emission that limits spectral resolution of thermodynamically desirable, decent energy gaps ΔE_{21} and makes an integration procedure challenging. An alternative approach to thermometry exploits the substantial differences in the time scales of total decay from the excited S_1 and T_1 states. In that case, ΔE_{21} can also be very low, which is an inherent strategy to enhance rISC in TADF emitters in general and a time-resolved thermometry readout concept can be envisioned. For the introduced simplified system containing two excited states coupled by ISC and rISC, the coupled rate equation system of those states reads

$$\begin{pmatrix}\dot{n}_1\\ \dot{n}_2\end{pmatrix} = \begin{pmatrix}-\left(k_1 + k_{nr}^{abs}(T)\right) & k_{nr}^{em}(T)\\ k_{nr}^{abs}(T) & -\left(k_2 + k_{nr}^{em}(T)\right)\end{pmatrix}\begin{pmatrix}n_1\\ n_2\end{pmatrix} + \begin{pmatrix}\alpha_{a1}Kn_a\\ \alpha_{a2}Kn_a\end{pmatrix} \tag{8}$$

with K as the total decay rate constant of the feeding state $|a\rangle$. For a temperature-dependent decay analysis, it is common to selectively pump into state $|2\rangle = S_1$ and analyze the prompt and delayed fluorescence as a function of temperature. This leads to condition $n_a = 0$, and the boundary condition

$$\begin{pmatrix}n_1\\ n_2\end{pmatrix}\Big|_{t-t_0=0} = \begin{pmatrix}0\\ n_0\end{pmatrix} \tag{9}$$

with n_0 as the initial population density in the S_1 state that is allowed to freely decay.

It should be noted that the excited state landscape of organic dyes is usually much more complex with many more singlet and triplet states. However, this does not readily affect the present analysis, which involves the radiatively decaying excited states being relevant for ratiometric thermometry. Those emissive states often are the lowest energetic ones given the validity

of Kasha's rule and fast internal conversion rates in the order of ps. Higher excited states or environment effects can have an indirect impact on the interconnecting nonradiative coupling rates. For example, it is well-established that the presence of excited states with localized charge density (often dubbed as local excited, LE) can significantly affect intrinsic ISC rates by means of spin-vibronic (Herzberg–Teller-type) coupling. In several organic TADF emitters, the lowest excited singlet state is of CT-type character, while the lowest excited triplet rather shows LE character, which enables ISC by means of El-Sayed's rules.[44] In addition, the energy of CT-type excited states often relevant in TADF emitters is also strongly affected by the polarity or dielectric properties of the surrounding environment. Very often do more polar environments stabilize such CT-type states, which does not only induce a bathochromically shifted emission but also has an indirect impact on the intrinsic ISC rates based on the energy difference to other LE states and perturbative spin-vibronic admixture that enhances ISC. This is often also helpful to enhance rISC then by lower crossover barriers (or reorganization energies in the Marcus–Jortner–Levich framework).[84,85]

Next to this intrinsic property, bathochromically shifted broad-band emission is usually much more prone to nonradiative relaxation by lower thermal crossover barriers (or reorganization energies in the framework of Marcus theory). This enhances the total decay rates k_1 and k_2 of the two lowest energetic excited states, which both mutual ISC and rISC have to compete with. Such a situation generally lowers the accessible dynamic temperature working range of a luminescent thermometer and needs to be carefully adjusted.[86]

With the boundary conditions set, it is instructive to consider solutions of eqn (8) under the boundary conditions (9) and discuss their use to extract (r)ISC rate constants.[87–90] In the context of this analysis, I will explicitly focus on the extraction of temperature dependences. For $n_a = 0$, eqn (8) is a homogeneous differential equation system and can be solved straightforwardly

$$\begin{pmatrix} n_1 \\ n_2 \end{pmatrix} = \frac{n_0}{\kappa_- - \kappa_+}\left[\begin{pmatrix} k_{nr}^{em} \\ K_1 + \kappa_- \end{pmatrix} e^{\kappa_-(t-t_0)} - \begin{pmatrix} k_{nr}^{em} \\ K_1 + \kappa_+ \end{pmatrix} e^{\kappa_+(t-t_0)}\right]. \tag{10}$$

where

$$\kappa_\pm = -\frac{1}{2}\left[(K_1 + K_2) \pm \sqrt{(K_2 - K_1)^2 + 4k_{nr}^{abs}k_{nr}^{em}}\right] \tag{11}$$

are the eigenvalues of the rate matrix in eqn (8) and $K_1 = k_1 + k_{nr}^{abs}$ and $K_2 = k_2 + k_{nr}^{em}$. The temperature dependence is dominantly involved in the nonradiative absorption (rISC) or emission (ISC) rates. It should also be noted that $\kappa_\pm < 0$. We can then identify the higher rate κ_+ with a negative prompt ($\kappa_+ = -k_p$) and the lower rate with a negative delayed component ($\kappa_- = -k_d$). It follows from eqn (11) that the excited S_1 state shows a biexponential decay with a prompt and delayed component, while the excited (lower energetic) T_1 state shows a rise with k_p followed by a decay with the delayed rate constant k_d.

Before we consider this most general case, it is very insightful to regard two limiting cases. The low temperature case, for which $k_{nr}^{abs} = k_{rISC} \to 0$, leads to $\kappa_+ = -k_p \to -K_2 = -(k_2 + k_{nr}^{em})$ and $\kappa_- = -k_d \to -k_1$ and thus,

$$\begin{pmatrix} n_1 \\ n_2 \end{pmatrix} = n_0\left[\begin{pmatrix} \frac{k_{nr}^{em}}{K_2 - k_1} \\ 0 \end{pmatrix} e^{-k_1(t-t_0)} + \begin{pmatrix} -\frac{k_{nr}^{em}}{K_2 - k_1} \\ 1 \end{pmatrix} e^{-K_2(t-t_0)}\right], \tag{12}$$

i.e. state $|2\rangle = S_1$ shows a single exponential decay with the rate constant $K_2 = k_p$, while state $|1\rangle = T_1$ decays with a rate constant $k_1 = k_d$ and is fed from S_1 with a rise component $K_2 = k_p$. In the limit of weak ISC ($k_{ISC} \ll k_2$ or $K_2 \approx k_2$), the S_1 and T_1 state decouple completely and given boundary condition (9), there would be no T_1 feeding at all. In that extreme, only prompt fluorescence from the excited S_1 state will be essentially detected.

It is now instructive to consider comparably weak, but non-negligible rISC, *i.e.* $k_{nr}^{abs} = k_{rISC} \ll k_{nr}^{em} = k_{ISC} \lesssim K_2$. Moreover, we assume that $K_1 \ll K_2$. The root in eqn (11) can then be expanded to first order and upon usage of the definition of a relative triplet feeding ratio,

$$\gamma_1 = \gamma_T = \frac{k_{nr}^{em}}{K_2} = \frac{k_{ISC}}{k_2 + k_{ISC}} \tag{13}$$

we find $k_p = K_2 + \gamma_1 k_{nr}^{abs} = K_2 + \gamma_T k_{rISC} \approx K_2$ and $k_d = K_1 - \gamma_1 k_{nr}^{abs} = k_1 + (1 - \gamma_T)k_{rISC}$. Both rate constants evolve to the previously described case in the limit of $k_{nr}^{abs} \to 0$. It becomes evident that in this weak coupling limit and upon usage of eqn (4), the prompt rate constant k_p remains virtually temperature-independent, while the delayed rate constant k_d increases with increasing temperature. Thus, measuring the delayed rate constant as a function of temperature can already serve as a thermometric measure in principle accordingo eqn (4), as has also been experimentally recorded before.[54,87] However, it is usually challenging to correctly connect the resulting energy gap from the fit to a spectroscopically verifiable value.

Within that weak coupling scheme, we can also derive the connected amplitudes to the prompt and delayed component using eqn (10)

$$\begin{pmatrix} n_1 \\ n_2 \end{pmatrix} \approx n_0\left[\begin{pmatrix} \gamma_1 \\ \gamma_1{}^2\frac{g_2}{g_1}\exp\left(-\frac{\Delta E_{21}}{k_B T}\right) \end{pmatrix} e^{-\left[k_1 + (1-\gamma_1)k_{nr}^{abs}\right](t-t_0)} + \begin{pmatrix} -\gamma_1 \\ 1 + \gamma_1{}^2\frac{g_2}{g_1}\exp\left(-\frac{\Delta E_{21}}{k_B T}\right) \end{pmatrix} e^{-\left[K_2 + \gamma_1 k_{nr}^{abs}\right](t-t_0)}\right] \tag{14}$$

Thus, the triplet state $|1\rangle = T_1$ shows a rise component with feeding rate constant $k_p = K_2 + \gamma_1 k_{nr}^{abs} \approx K_2$ and a decay with temperature-dependent delayed component $k_d = k_1 + (1 - \gamma_1)k_{nr}^{abs}$ with essentially temperature-independent amplitude. In contrast, the singlet state $|2\rangle = S_1$ shows a biexponential decay with temperature-dependent prompt (A_p) and delayed (A_d) amplitudes. Thus, next to the delayed rate constant k_d, also its

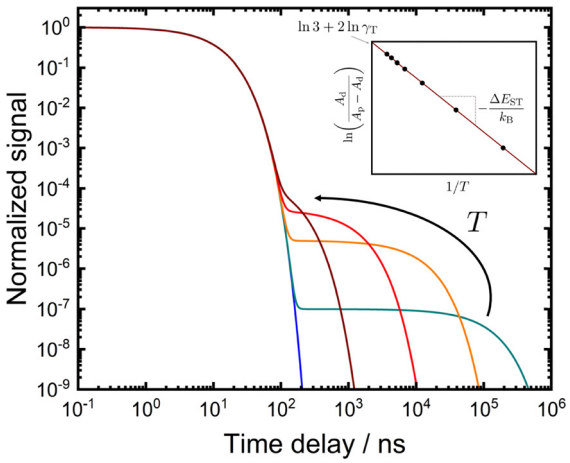

Fig. 3 Schematic temperature-dependent decay curves of the excited singlet state S_1 of a typical TADF emitter within the weak coupling scheme (k_p = 0.1 ns^{-1}, k_d in µs^{-1} range). The inset depicts the behavior of the amplitude of the delayed component according to eqn (15) that could be used to calibrate the emitter for ratiometric thermometry in the time domain.

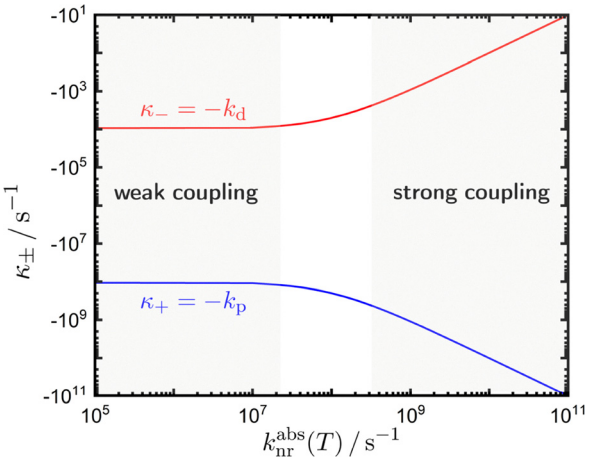

Fig. 4 Evolution of the two excited state rate constants $\kappa_\pm$ with the rate-determining constant $k_{nr}^{abs}(T)$ that can be envisioned as a coupling strength between the two excited states $|1\rangle$ and $|2\rangle$. Exemplary values were k_1 = 10 ms^{-1} and K_2 = 0.1 ns^{-1} (for definitions see text) representative for a TADF emitter. Most practical TADF emitters tend to be in the weak coupling regime. Inorganic emitters such as the lanthanoid ions or Cr^{3+} are much more commonly in the strong coupling regime at ambient temperatures, which is relevant to ratiometric thermometry with steady-state spectra.

amplitude could be considered as a temperature measure that increases with temperature and shows Boltzmann behavior. It is instructive to verify that eqn (14) evolves to eqn (12) in the limit of $k_{nr}^{abs} \to 0$ (assuming $K_1 \ll K_2$). Thus, not only may k_d serve as a temperature-dependent measure but also the amplitudes A_p and A_d. A reasonable and well-defined (even at $T \to 0$) ratiometric definition for that limit is

$$\frac{A_d}{A_p - A_d} = \gamma_1^2 \frac{g_2}{g_1} \exp\left(-\frac{\Delta E_{21}}{k_B T}\right) \tag{15}$$

Thus, the as-defined amplitude ratio offers an alternative way for ratiometric Boltzmann thermometry in the time domain (see Fig. 3). It should be noted that this approach does, however, necessarily imply that rISC is comparably weak and the rate-determining step. Experimentally, this approach will usually require the use of intensified charge-couple device (iCCD) cameras that target wide dynamic working ranges and are optimized for light detection rather than timing resolution itself, for which time-correlated single-photon counting (TCSPC) and multi-channel scaling (MCS) techniques are usually the better choice. The qualitative agreement between the predictions from eqn (15) (see Fig. 3) and experimental data strongly confirms the robustness of this model despite the simplified view on only the radiatively emitting excited states. More selective data will have to be acquired experimentally to test the model and judge the quality of its assumptions.

Based on eqn (15), the relative sensitivity $S_r(T)$ can be defined as[2,3]

$$S_r(T) = \left|\frac{1}{f(T)}\frac{df}{dT}\right| = \frac{\Delta E_{21}}{k_B T^2} \tag{16}$$

just like for a conventional Boltzmann thermometer. The overall relative statistical uncertainty is[2,3]

$$\frac{\sigma_T}{T} = \pm\frac{T}{S_r(T)}\frac{\sigma_f(T)}{f(T)} = \pm\frac{k_B T}{\Delta E_{21}}\sqrt{\left(\frac{\sigma_p}{A_p}\right)^2 + \left(\frac{\sigma_d}{A_d}\right)^2} \tag{17}$$

where σ_p and σ_d are the statistical uncertainties of the amplitudes A_p and A_d in the time-resolved experiment, respectively, which depend on the explicit type of detection.[26]

Another insightful limit is the case of $k_{1,2} \ll k_{nr}(0)$, which will be referred to as the strong coupling limit (see Fig. 4). This is particularly given if intrinsic ISC is rather strong and there is perturbative admixture of the S_1 and T_1 state. In that limit, eqn (10) evolves to

$$\begin{pmatrix} n_1 \\ n_2 \end{pmatrix} = \frac{n_0}{k_{nr}^{em} + k_{nr}^{abs}}\left[\begin{pmatrix} k_{nr}^{em} \\ k_{nr}^{abs} \end{pmatrix} e^{-\langle k\rangle (t-t_0)} + \begin{pmatrix} -k_{nr}^{em} \\ k_{nr}^{em} \end{pmatrix} e^{-\left(\langle k\rangle + k_{nr}^{em} + k_{nr}^{abs}\right)(t-t_0)}\right] \tag{18}$$

with $k = \frac{1}{2}(k_1 + k_2)$. If we make use of approximations (3) and (4), we finally obtain

$$\begin{pmatrix} n_1 \\ n_2 \end{pmatrix} = \frac{n_0}{1 + \frac{g_2}{g_1}\exp\left(-\frac{\Delta E_{21}}{k_B T}\right)}\left[\begin{pmatrix} 1 \\ \frac{g_2}{g_1}\exp\left(-\frac{\Delta E_{21}}{k_B T}\right) \end{pmatrix} e^{-k(t-t_0)} + \begin{pmatrix} -1 \\ 1 \end{pmatrix} e^{-\left[k + k_{nr}^{em}\left(1 + \frac{g_2}{g_1}\exp\left(-\frac{\Delta E_{21}}{k_B T}\right)\right)\right](t-t_0)}\right] \tag{19}$$

Two limiting domains can be identified. If $\Delta E_{21} \gg k_B T$, state $|2\rangle = S_1$ essentially only shows single-exponential decay with the decay rate $k_p = k + k_{nr}^{em}$ since intrinsic coupling among the excited levels becomes so strong that they essentially

behave like an effective average single level. This situation is very often encountered for trivalent lanthanoid ions with coupled $4f^n$ spin–orbit levels. If, on the other hand, $\Delta E_{21} \ll k_B T$, it shows biexponential decay with $k_p = k + k_{nr}^{em} + k_{nr}^{abs}$ and $k_d = k$. For organic emitters, this situation is rather rare but can be encountered in several aromatic ketones as indicated above.[53,65] Alternatively, other mechanisms such as spin-vibronic or vibrational spin–orbit coupling may enhance the intrinsic intersystem crossing rate.[46–53] In that case, however, (steady-state) ratiometric thermometry in the spectral domain becomes a realistic alternative. However, most practically available TADF emitters are typically within the weak coupling limit, for which rISC is the rate-determining step at ambient temperatures.

Guidelines

The previous analysis demonstrates that ratiometric luminescent thermometry with practical TADF emitters should be ideally performed in a time domain with temperature-dependent time-resolved data. Besides the temperature evolution of the delayed component, k_d, the amplitude ratio of the prompt and delayed component according to eqn (15) is a useful measure for temperature. It is important that the analysis requires weak coupling ($k_{nr}^{abs} = k_{rISC} \ll k_{nr}^{em} = k_{ISC} \lesssim K_2$) between the relevant excited triplet and singlet state. This situation is particularly often given for donor–acceptor-type TADF emitters, in which there is a dominant charge transfer-type character of both excited states and LE states do not lead to significant admixtures by means of Herzberg–Teller coupling to ensure sufficiently low intrinsic ISC rates $k_{ISC}(0)$.[46,50,53] On the other hand, $k_{ISC}(0)$ must also not be too low to avoid an overly low γ_T that affects the overall achievable precision (see eqn (15)).

From a thermodynamic perspective, it is still recommendable that $\Delta E_{21} = \Delta E_{ST}$ is in the optimum range derived for any ratiometrically working thermometer,[3]

$$\Delta E_{21} \in \left[2k_B T_{opt}, \left(2+\sqrt{2}\right)k_B T_{opt}\right] \quad (20)$$

to ensure a reasonable compromise between high relative sensitivity of the ratiometric thermometer and appreciable signal-to-noise from both amplitudes (see also eqn (17)).

Conclusions

Unlike their inorganic single-ion emitter counterparts, TADF emitters are so far only scarcely considered for ratiometric luminescent thermometry despite their prominent temperature-dependent luminescence. Within this work, reasons for this empirical fact are elucidated analyzing the temperature-dependent excited state dynamics of an idealized three-level system. It is elaborated that conventional ratiometric thermometry in a spectral domain essentially only works well in case of sufficiently strong intrinsic coupling between the two excited states. While this is common for many inorganic emitters (trivalent lanthanoid ions with $4f^n \leftrightarrow 4f^n$ transitions, Sm^{2+}, Pr^{3+} with a $4f^{n-1}5d^1 \leftrightarrow 4f^2$ transition or Cr^{3+} with $3d^3 \leftrightarrow 3d^3$ transitions in octahedral ligand fields), organic emitters usually suffer from comparably slow (r)ISC compared to the total decay of the two excited levels that limits their kinetically enabled thermalization. Moreover, the broad-band appearance of both fluorescent and phosphorescent emission poses practical problems if energy gaps in the order of $k_B T$ are to be resolved. However, aromatic ketones or recently evolved Zn(II) complexes could be possible alternative candidates. In contrast, an alternative time-resolved ratiometric approach is proposed. For that purpose, different coupling schemes are discussed as limiting cases for the exact temperature-dependent kinetics of a three-level system. It is demonstrated how the strong coupling scheme typically valid for the previously mentioned inorganic emitters evolves and how ratiometric thermometry could be performed as is often the case for TADF emitters. It is based on the amplitudes of the fast and slow component of the biexponential decay of the luminescence intensity of the excited singlet state in case of weak mutual coupling of the excited states. Overall, it turns out that appropriate design of TADF emitters for ratiometric thermometry requires a fundamental understanding on how to control intersystem crossing between the excited singlet and triplet state – a topic that Christel Marian has contributed a lot to with her theoretical insights beyond the Franck–Condon limit.

Conflicts of interest

There are no conflicts to declare.

Data availability

No primary research results, software or code have been included and no new data were generated or analysed as part of this article.

Acknowledgements

Financial support by a materials cost allowance of the Fonds der Chemischen Industrie e.V. and the ''Young College'' of the North-Rhine Westphalian Academy of Sciences, Humanities, and the Arts is gratefully acknowledged by the author. The author wants to explicitly thank Christel Marian for ever enlightening and joyful discussions at a cup of coffee or tea, her continuous support, and constant interest in the author's works. The members of the Research Training Group ModISC (GRK 2482, project no. 396890929) funded by the German National Research Foundation (DFG) for their interest in the author's works are additionally gratefully acknowledged.

References

1 S. A. Wade, S. F. Collins and G. W. Baxter, *J. Appl. Phys.*, 2003, **94**, 4743–4756.
2 C. D. S. Brites, R. Marin, M. Suta, A. N. C. Neto, E. Ximendes, D. Jaque and L. D. Carlos, *Adv. Mater.*, 2023, **35**, 2302749.
3 M. Suta and A. Meijerink, *Adv. Theory Simul.*, 2020, **3**, 2000176.

4 C. D. S. Brites, S. Balabhadra and L. D. Carlos, *Adv. Opt. Mater.*, 2019, **7**, 1801239.
5 Z. Cao, X. Wie, L. Zhao, Y. Chen and M. Yin, *ACS Appl. Mater. Interfaces*, 2016, **8**, 34546–34551.
6 B. Bendel and M. Suta, *J. Mater. Chem. C*, 2022, **10**, 13805–13814.
7 L. Cui, Z. Dong, D. Yu, Y. Wang and A. Meijerink, *Sci. Adv.*, 2024, **10**, eado7737.
8 C. D. S. Brites, K. Fiaczyk, J. F. C. B. Ramalho, M. Sójka, L. D. Carlos and E. Zych, *Adv. Opt. Mater.*, 2018, **6**, 1701318.
9 M. Sójka, J. F. C. B. Ramalho, C. D. S. Brites, K. Fiaczyk, L. D. Carlos and E. Zych, *Adv. Opt. Mater.*, 2019, **7**, 1901102.
10 M. Sójka, C. D. S. Brites and E. Zych, *J. Mater. Chem. C*, 2020, **8**, 10086–10097.
11 P. Bolek, J. Zeler, C. D. S. Brites, J. Trojan-Piegza, L. D. Carlos and E. Zych, *Chem. Eng. J.*, 2021, **421**, 129764.
12 M. Sójka, W. Piotrowski, L. Marciniak and E. Zych, *J. Alloys Compd.*, 2024, **970**, 172662.
13 P. Bolek, T. van Swieten, J. Zeler, A. Meijerink and E. Zych, *Chem. Mater.*, 2024, **36**, 8894–8909.
14 M. Back, E. Trave, J. Ueda and S. Tanabe, *Chem. Mater.*, 2016, **28**, 8347–8356.
15 M. Back, J. Ueda, M. G. Brik, T. Lesniewski, M. Grinberg and S. Tanabe, *ACS Appl. Mater. Interfaces*, 2018, **10**, 41512–41524.
16 J. Ueda, M. Back, M. G. Brik, Y. Zhuang, M. Grinberg and S. Tanabe, *Opt. Mater.*, 2018, **85**, 510–516.
17 M. Back, J. Ueda, J. Xu, K. Asami, M. G. Brik and S. Tanabe, *Adv. Opt. Mater.*, 2020, **8**, 2000124.
18 M. Back, J. Ueda, M. G. Brik and S. Tanabe, *ACS Appl. Mater. Interfaces*, 2020, **12**, 38325–38332.
19 M. Back, J. Ueda, H. Nambu, M. Fujita, A. Yamamoto, H. Yoshida, H. Tanaka, M. G. Brik and S. Tanabe, *Adv. Opt. Mater.*, 2021, **9**, 2100033.
20 K. Elzbieciak-Piecka, M. Suta and L. Marciniak, *Chem. Eng. J.*, 2021, **421**, 129757.
21 Z. Ristić, V. Đorđević, M. Medić, S. Kuzman, M. Sekulić, Ž. Antić and M. D. Dramićanin, *Meas. Sci. Technol.*, 2021, **32**, 054004.
22 K. Elzbieciak-Piecka and L. Marciniak, *Sci. Rep.*, 2022, **12**, 16364.
23 M. Szymczak, A. Antuzevics, P. Rodionovs, M. Runowski, U. R. Rodríguez-Mendoza, D. Szymanski, V. Kinzhybalo and L. Marciniak, *ACS Appl. Mater. Interfaces*, 2024, **16**, 64976–64987.
24 E. Andreato, N. Panov, A. Artiga, V. Osipova, U. Resch-Genger, E. Ximendes, P. Molina, P. Canton and R. Marin, *Chem. Mater.*, 2025, **37**, 3197–3210.
25 M. Suta, *Opt. Mater.: X*, 2022, **16**, 100195.
26 T. P. van Swieten, A. Meijerink and F. T. Rabouw, *ACS Photonics*, 2022, **9**, 1366–1374.
27 J. M. dos Santos, D. Hall, B. Basumatary, M. Bryden, D. Chen, P. Choudhary, T. Comerford, E. Crovini, A. Danos, J. De, S. Diesing, M. Fatahi, M. Griffin, A. K. Gupta, H. Hafeez, L. Hämmerling, E. Hanover, J. Haug, T. Heil, D. Karthik, S. Kumar, O. Lee, H. Li, F. Lucas, C. F. R. Mackenzie, A. Mariko, T. Matulaitis, F. Millward, Y. Olivier, Q. Qi, I. D. W. Samuel, N. Sharma, C. Si, L. Spierling, P. Sudhakar, D. Sun, E. Tankelevičiūte, M. D. Tonet, J. Wang, T. Wang, S. Wu, Y. Xu, L. Zhang and E. Zysman-Colman, *Chem. Rev.*, 2024, **124**, 13736–14110.
28 F. Perrin, *Ann. Phys.*, 1929, **12**, 169–275.
29 G. N. Lewis, D. Lipkin and T. T. Magel, *J. Am. Chem. Soc.*, 1941, **63**, 3005–3018.
30 C. A. Parker and C. G. Hatchard, *Trans. Faraday Soc.*, 1961, **57**, 1894–1904.
31 C. A. Parker and T. A. Joyce, *Chem. Commun.*, 1968, 1421–1422.
32 H. Uoyama, K. Goushi, K. Shizu, H. Nomura and C. Adachi, *Nature*, 2012, **492**, 234–238.
33 P. Data, P. Pander, M. Okazaki, Y. Takeda, S. Minakata and A. P. Monkman, *Angew. Chem., Int. Ed.*, 2016, **55**, 5739–5744.
34 L.-S. Cui, A. J. Gillett, S.-F. Zhang, H. Ye, Y. Liu, X.-K. Chen, Z.-S. Lin, E. W. Evans, W. K. Myers, T. K. Ronson, H. Nakanotani, S. Reineke, J.-L. Bredas, C. Adachi and R. H. Friend, *Nat. Photonics*, 2020, **14**, 636–642.
35 C.-Y. Chan, M. Tanaka, Y.-T. Lee, Y.-W. Wong, H. Nakanotani, T. Hatakeyama and C. Adachi, *Nat. Photonics*, 2021, **15**, 203–205.
36 T. Hatakeyama, K. Shiren, K. Nakajima, S. Nomura, S. Nakatsuka, K. Kinoshita, J. Ni, Y. Ono and T. Ikuta, *Adv. Mater.*, 2016, **28**, 2777–2781.
37 Y. Kondo, K. Yoshiura, S. Kitera, H. Nishi, S. Oda, H. Gotoh, Y. Sasada, M. Yanai and T. Hatakeyama, *Nat. Photonics*, 2019, **13**, 678–682.
38 D. H. Ahn, S. W. Kim, H. Lee, I. J. Ko, D. Karthik, J. Y. Lee and J. H. Kwon, *Nat. Photonics*, 2019, **13**, 540–546.
39 D. Hall, S. M. Suresh, P. L. dos Santos, E. Duda, S. Bagnich, A. Pershin, P. Rajamalli, D. B. Cordes, A. M. Z. Slawin, D. Beljonne, A. Köhler, I. D. W. Samuel, Y. Olivier and E. Zysman-Colman, *Adv. Opt. Mater.*, 2020, **8**, 1901627.
40 H. Tanaka, S. Oda, G. Ricci, H. Gotoh, K. Tabata, R. Kawasumi, D. Beljonne, Y. Oliver and T. Hatakeyama, *Angew. Chem., Int. Ed.*, 2021, **60**, 17910–17914.
41 S. Wu, L. Zhang, J. Wang, A. K. Gupta, I. D. W. Samuel and E. Zysman-Colman, *Angew. Chem., Int. Ed.*, 2023, **62**, e202305182.
42 Y. Wada, H. Nakagawa, S. Matsumoto, Y. Wakisaka and H. Kaji, *Nat. Photonics*, 2020, **14**, 643–649.
43 N. Aizawa, Y.-J. Pu, Y. Harabuchi, A. Nihonyanagi, R. Ibuka, H. Inuzuka, B. Dhara, Y. Koyama, K. Nakayama, S. Maeda, F. Araoka and D. Miyajima, *Nature*, 2022, **609**, 502–506.
44 M. A. El-Sayed, *J. Chem. Phys.*, 1963, **38**, 2834–2838.
45 B. T. Lim, S. Okajima, A. K. Chandra and E. C. Lim, *Chem. Phys. Lett.*, 1981, **79**, 22–27.
46 M. K. Etherington, J. Gibson, H. F. Higginbotham, T. J. Penfold and A. P. Monkman, *Nat. Commun.*, 2016, **7**, 13680.
47 J. Gibson, A. P. Monkman and T. J. Penfold, *ChemPhysChem*, 2016, **17**, 2956–2961.
48 J. Gibson and T. J. Penfold, *Phys. Chem. Chem. Phys.*, 2017, **19**, 8428–8434.

49 P. K. Samanta, D. Kim, V. Coropceanu and J.-L. Brédas, *J. Am. Chem. Soc.*, 2017, **139**, 4042–4051.
50 T. J. Penfold, E. Gindensperger, C. Daniel and C. M. Marian, *Chem. Rev.*, 2018, **118**, 6975–7025.
51 C. M. Marian, *J. Phys. Chem. C*, 2016, **120**, 3715–3721.
52 I. Lyskov and C. M. Marian, *J. Phys. Chem. C*, 2017, **121**, 21145–21153.
53 C. M. Marian, *Ann. Rev. Phys. Chem.*, 2021, **72**, 617–640.
54 J. C. Fister, D. Rank and J. M. Harris, *Anal. Chem.*, 1995, **67**, 4269–4275.
55 C. Baleizão, S. Nagl, S. M. Borisov, M. Schäferling, O. S. Wolfbeis and M. N. Berberan-Santos, *Chem. – Eur. J.*, 2007, **13**, 3643–3651.
56 V. Augusto, C. Baleizão, M. N. Berberan-Santos and J. P. S. Farinha, *J. Mater. Chem.*, 2010, **20**, 1192–1197.
57 A. Steinegger, I. Klimant and S. M. Borisov, *Adv. Opt. Mater.*, 2017, **5**, 1700372.
58 A. Steinegger and S. M. Borisov, *ACS Omega*, 2020, **5**, 7729–7737.
59 R. G. Geitenbeek, H. W. de Wijn and A. Meijerink, *Phys. Rev. Appl.*, 2018, **10**, 064006.
60 R. Czerwieniec, M. J. Leitl, H. H. H. Homeier and H. Yersin, *Coord. Chem. Rev.*, 2016, **325**, 2–28.
61 R. Hamze, J. L. Peltier, D. Sylvinson, M. Jung, J. Cardenas, R. Haiges, M. Soleilhavoup, R. Jazzar, P. I. Djurovich, G. Bertrand and M. E. Thompson, *Science*, 2019, **363**, 601–606.
62 J. Guhl, D. Sretenović, P. Schmeinck, S. Felekyan, R. Kühnemuth, C. Ganter, C. A. M. Seidel, C. M. Marian and M. Suta, *J. Mater. Chem. C*, 2024, **12**, 10036–10052.
63 T.-Y. Li, S.-J. Zheng, P. I. Djurovich and M. E. Thompson, *Chem. Rev.*, 2024, **124**, 4332–4392.
64 H. Yersin, A. F. Rausch, R. Czerwieniec, T. Hofbeck and T. Fischer, *Coord. Chem. Rev.*, 2011, **255**, 2622–2652.
65 S. Metz and C. M. Marian, *ChemPhotoChem*, 2022, **6**, e202200098.
66 N. Lüdtke, A. Steffen and C. M. Marian, *Inorg. Chem.*, 2022, **61**, 20896–20905.
67 N. Lüdtke, J. Kuhnt, T. Heil, A. Steffen and C. M. Marian, *ChemPhotoChem*, 2023, **7**, e202200142.
68 O. Mrózek, M. Mitra, B. Hupp, A. Belyaev, N. Lüdtke, D. Wagner, C. Wang, O. S. Wenger, C. M. Marian and A. Steffen, *Chem. – Eur. J.*, 2023, **29**, e202203980.
69 M. Mitra, O. Mrózek, M. Putscher, J. Guhl, B. Hupp, A. Belyaev, C. M. Marian and A. Steffen, *Angew. Chem., Int. Ed.*, 2024, **63**, e202316300.
70 J. Kuhnt, M. Mitra, S. Maity, B. Hupp, C. M. Marian and A. Steffen, *J. Phys. Chem. Lett.*, 2024, **15**, 6409–6414.
71 J. C. Dalton and F. C. Montgomery, *J. Am. Chem. Soc.*, 1974, **96**, 6230–6232.
72 J. J. Cavaleri, K. Prater and R. M. Bowman, *Chem. Phys. Lett.*, 1996, **259**, 495–502.
73 B. Heinz, B. Schmidt, C. Root, H. Satzger, F. Milota, B. Fierz, T. Kiefhaber, W. Zinth and P. Gilch, *Phys. Chem. Chem. Phys.*, 2006, **8**, 3432–3439.
74 S. Salzmann, J. Tatchen and C. M. Marian, *J. Photochem. Photobiol., A*, 2008, **198**, 221–231.
75 V. Rai-Constapel, S. Salzmann and C. M. Marian, *J. Phys. Chem. A*, 2011, **115**, 8589–8596.
76 V. Rai-Constapel, M. Etinski and C. M. Marian, *J. Phys. Chem. A*, 2013, **117**, 3935–3944.
77 T. Villnow, G. Ryseck, V. Rai-Constapel, C. M. Marian and P. Gilch, *J. Phys. Chem. A*, 2014, **118**, 11696–11707.
78 V. Rai-Constapel, T. Villnow, G. Ryseck, P. Gilch and C. M. Marian, *J. Phys. Chem. A*, 2014, **118**, 11708–11717.
79 M. Bracker, F. Dinkelbach, O. Weingart and M. Kleinschmidt, *Phys. Chem. Chem. Phys.*, 2019, **21**, 9912–9923.
80 K. A. Thom, F. Wieser, K. Diestelhorst, A. Reiffers, C. Czekelius, M. Kleinschmidt, M. Bracker, C. M. Marian and P. Gilch, *J. Phys. Chem. Lett.*, 2021, **12**, 5703–5709.
81 M. Bracker, M. K. Kubitz, C. Czekelius, C. M. Marian and M. Kleinschmidt, *ChemPhotoChem*, 2022, **6**, e2022200040.
82 S. Metz and C. M. Marian, *ChemPhotoChem*, 2022, **6**, e202200098.
83 M. Jantz, D. Klaverklamp, L. Bunnemann, M. Kleinschmidt, C. Czekelius and P. Gilch, *Phys. Chem. Chem. Phys.*, 2025, **27**, 10444–10455.
84 R. A. Marcus, *J. Chem. Phys.*, 1956, **24**, 966–978.
85 J. Ulstrup and J. Jortner, *J. Chem. Phys.*, 1975, **63**, 4358–4368.
86 A. J. Gillett, A. Pershin, R. Pandya, S. Feldmann, A. J. Sneyd, A. M. Alvertis, E. W. Evans, T. H. Thomas, L.-S. Cui, B. H. Drummond, G. D. Scholes, Y. Olivier, A. Rao, R. H. Friend and D. Beljonne, *Nat. Mater.*, 2022, **21**, 1150–1157.
87 F. B. Dias, T. J. Penfold and A. P. Monkman, *Methods Appl. Fluoresc.*, 2017, **5**, 012001.
88 N. Haase, A. Danos, C. Pflumm, A. Morherr, P. Stachelek, A. Mekic, W. Brütting and A. P. Monkman, *J. Phys. Chem. C*, 2018, **122**, 29173–29179.
89 Y. Tsuchiya, S. Diesing, F. Bencheikh, Y. Wada, P. L. dos Santos, H. Kaji, E. Zysman-Colman, I. D. W. Samuel and C. Adachi, *J. Phys. Chem. A*, 2021, **125**, 8074–8089.
90 S. Sem, S. Jenatsch, K. Stavrou, A. Danos, A. P. Monkman and B. Ruhstaller, *J. Mater. Chem. C*, 2022, **10**, 4878–4885.

